The usability of the Judd-Ofelt theory for luminescent thermometry using Eu^{3+}-doped phosphate glass

*Bartosz Bondzior** [a,b], *Chi Nguyen* [b], *Thi Hong Quan Vu* [a], *Diego Pugliese* [c], *Przemysław J. Dereń* [a], *Laeticia Petit* [b]

[a] Institute of Low Temperature and Structure Research, Polish Academy of Sciences, Okólna 2, 50-422 Wrocław, Poland

[b] Laboratory of Photonics, Tampere University, Korkeakoulunkatu 3, 33720 Tampere, Finland

[c] Department of Applied Science and Technology (DISAT) and INSTM RU, Politecnico di Torino, Corso Duca degli Abruzzi 24, 10129 Torino, Italy

* corresponding author: b.bondzior@intibs.pl

Keywords: glass, europium, luminescence, Judd-Ofelt theory

Abstract

The Judd-Ofelt theory, which is the most thorough and insightful method to determine theoretically the luminescent properties of the trivalent rare earth dopants, is here tested on Eu^{3+}-doped glasses in the P_2O_5 – SrO – CaO – Na_2O system to assess their usefulness as luminescent thermometers. It is demonstrated that the thermometric sensitivity (change of the emission lines ratio in response to change in temperature) can be estimated using the Judd-Ofelt theory and aligns well with the experimentally obtained values. It is shown here that the addition of B_2O_3 or SiO_2 in a phosphate network increases the absolute sensitivity due to an increase in the phosphate network connectivity while having no significant impact on the site of Eu^{3+} ions. The applicability of the Judd-Ofelt theory for predicting the thermometric parameters of a glass luminescent material, without the time-consuming measurement of the glasses spectroscopic

properties as a function of temperature, is clearly demonstrated and allows for further development of novel efficient luminescent thermal sensors with high sensitivity.

1. Introduction

The rising interest in the topic of luminescent thermometry over the recent years is driven by its application in biomedicine, photonics and nano-science.[1] Many research groups currently compete for the highest achieved sensitivity of the luminescent thermometer, defined as the largest change of the luminescence characteristics in response to a change in temperature.[2–4] As the sensitivity of a luminescent thermometer varies depending on the mode of temperature readout (band shape, peak emission intensity, decay time or rise time), it is quite challenging to compare the sensitivity performances of different materials reported in the literature. Nonetheless, the most popular readout mode to characterize luminescent thermometers is the fluorescence intensity ratio (FIR), where the thermometric signal is an intensity ratio of emission lines originating either from a single dopant, co-dopants or the host and a dopant.[5–7]

The majority of the materials studied for potential applications in luminescent thermometry are organic dyes,[8] polycrystalline powders[9,10] or core-shell nanoparticles (NPs).[11,12] For example, the organic dye *Escherichia coli* DH5α strains (Its265) reach relative sensitivity of 19.6% K^{-1} (at T = 318 K).[13] Polycrystalline Ho,Yb:Y_2O_3 and core-shell cubic $LiLuF_4$:Er,Yb@$LiLuF_4$ NPs exhibit relative sensitivity of 9.7% K^{-1} (at T = 85 K)[14] and 1.28% K^{-1} (at T = 303 K),[11] respectively. However, it is interesting to point out that very few glass-based materials have been tested for application as luminescent thermometers. For example, Eu^{3+}-doped $60(NaPO_3)_3$ + $35Al(PO_3)_3$ glass was reported with a relative sensitivity of 1.68% K^{-1} (at T = 288 K).[15]

Many attempts have been carried out on recent years to improve the thermometric sensitivity of a luminescent material: either by adjusting the composition and so the crystal field strength

in the dopants coordination sphere[6,16,17] or by changing the grain size of the nanocrystal and so the heat dissipation.[18] For example, improvement in thermometric response was achieved by means of phosphor mixing (32%),[19] modifying the covalency of the RE^{3+}-O^{2-} bond in nanocrystalline orthophosphates (30%)[20] or by increasing the Tb^{3+} concentration in TZPN glass (28%).[21] It is, however, not as effective as tuning the size of the thermometric NPs (138%)[22] or co-doping with transition metal ions (300%).[23]

For many decades, the Judd-Ofelt (J-O) theory has been used to investigate the structural changes occurring in the luminescent material from the variation in three parameters: Ω_2, Ω_4, and Ω_6. The first parameter Ω_2 depends mainly on the symmetry of the material, while the latter two Ω_4 and Ω_6 can be related to the covalency of the bonds.[24] The J-O theory was used in the investigation of glasses in the 90's, but most of the research addressed the Er^{3+}- and Pr^{3+}-doped materials.[25–27] There are fewer papers on the J-O parameters derived from the Eu^{3+}-doped glasses,[28] and to the best of our knowledge, no such study has been reported on any glasses in the P_2O_5 – SrO – CaO – Na_2O system, which otherwise was subject of studies on the impact of composition modification on luminescent properties [29,30].

Recently, the J-O theory was demonstrated to be useful to gain insight regarding the crucial factors impacting the thermometric performance.[31] This method takes a classic approach to luminescent thermometry based on two thermally coupled excited levels – in the case of Eu^{3+} these levels are usually $^5D_0$ and $^5D_1$. Since the occupation of these excited levels is governed by the Boltzmann statistics, the relative intensity of emission from these levels is used to determine the FIR and serves as a thermometric variable.[32] Since the J-O parameters depend on the composition and structure of the host material, it is reasonable to expect that changes in the composition influence the luminescent properties of the materials. Therefore, knowing the impact of the compositional modification on the J-O parameters, the FIR from luminescent thermometer can be predicted as demonstrated in recent studies.[29,31] Surprisingly, to the best of our knowledge, there have been yet no attempts on predicting the thermometric performance of

luminescence temperature sensor based on glass from its spectroscopic properties. The only efforts were focused on crystalline powders e.g. $Y_2O_3:Eu^{3+}$ single crystals.[33]

Consequently, in this paper, the utilization of the J-O theory for optimization of the luminescent temperature sensor performance is put to test on Eu^{3+}-doped phosphate glasses. The J-O parameters are determined from the spectroscopic properties of glasses and are used to calculate the thermometric properties of the glasses which are compared with the experimentally obtained results. Besides that, the influence of adding SiO_2 or B_2O_3 on the thermometric properties of the phosphate glass is reported in order to understand the relation between glass composition and thermometric performance which is crucial for the development of new temperature sensors with enhanced thermal sensitivity.

2. Materials and Methods

2.1 Glass preparation

Glasses with the composition (in mol%) $(50\text{-}x)P_2O_5$ - $xSiO_2/B_2O_3$ - 20SrO - 20CaO -$10Na_2O$, with x = (0, 2.5 and 5 mol%), were prepared through a standard melt-quenching process in normal atmosphere. All the glasses were prepared with a fixed amount of Eu_2O_3, set at 1 mol%, and the amount of the rest of the elements were adjusted to 99%. The glass with $x = 0$ is referred as REF. The glasses with 2.5 and 5 mol% SiO_2 are labeled as Si-2.5 and Si-5, respectively, while the glasses with 2.5 and 5 mol% B_2O_3 are labeled as B-2.5 and B-5, respectively. The glasses were prepared using $NaPO_3$ (Alfa Aesar, tech.), $SrCO_3$ (Sigma-Aldrich, ≥98%), $Ca(PO_3)_2$, Eu_2O_3 (Sigma-Aldrich, ≥99.9%), NH_6PO_4 (Sigma-Aldrich, ≥99.5%), H_3BO_3 (Sigma-Aldrich, ≥99.5%) and SiO_2 (Umicore, 99.99%).

$Ca(PO_3)_2$ precursor was independently prepared using $CaCO_3$ (Sigma-Aldrich, ≥98%) and $(NH_4)_2HPO_4$ (Sigma-Aldrich, ≥99%) as raw materials and with a heating up to 850 °C with intermittent stages for 50 h.

The 10 g batches were melted in a platinum crucible from 1100 to 1475 °C, depending on the glass composition. After quenching, the glasses were annealed at 40 °C below their glass transition temperature for 6 h to decrease their residual stress. After annealing, all the glasses were cut and optically polished or ground into powder, depending on the characterization technique.

2.2 Characterization

The glass transition temperature (T_g) and crystallization temperature (T_p) were measured by differential thermal analysis (DTA) using a Netszch JUPITER F1 instrument. The measurement was carried out in a Pt crucible at a heating rate of 10 °C/min. T_g was determined as the inflection point of the endotherm obtained by taking the first derivative of the DTA curve, while T_p was taken as the maximum peak of the exotherm. T_x corresponds to the onset of the crystallization peak. All temperatures are given with an error of ± 3 °C.

The density of the glasses was measured using Archimedes' method with an accuracy of ± 0.02 g/cm^3, using ethanol as immersion fluid.

The structural properties of the glasses were assessed using Fourier Transform Infrared (FTIR) spectroscopy, in Attenuated Total Reflection mode (FTIR-ATR). FTIR-ATR spectra were acquired on glass powders with a Spectrum Two FT-IR Spectrometer. The spectra were recorded in the range from 620 to 1400 cm^{-1} and were normalized to the band with maximum intensity (~880 cm^{-1}).

The refractive index (n) was measured at five different wavelengths, namely 633, 825, 1061, 1312 and 1533 nm, with a fully automated Metricon 2010 prism-coupler refractometer. The accuracy of the measurement was estimated to ± 0.001.

The excitation and emission spectra were recorded using the Edinburgh Instruments FLS 1000 equipped with a Xenon lamp and a 550 nm long pass filter. The emission decay times were also measured using Edinburgh Instruments FLS 1000 and a microsecond flash lamp.

The luminescence measurements as a function of temperature were conducted using Linkam THMS 600 Heating/Freezing Stage (The McCRONE group, Westmont, IL USA), a 375 nm laser diode as an excitation source and the Hamamatsu Photonic multichannel analyzer PMA-12 equipped with a BT-CCD linear image sensor (Hamamatsu Photonics K.K, Shizuoka, Japan). The quantum yield (QY) was measured using the Hamamatsu PMA-12 spectrophotometer equipped with an integrating sphere. The accuracy of measurement is estimated to be ± 10%. The decay time curves were recorded using LeCroy digital oscilloscope and a Nd:YAG laser with Ti-Sapphire extension at 395 nm. The mean decay times were calculated from Eq. (1):

$$\langle \tau \rangle = \frac{\int t \cdot I(t) dt}{\int I(t) dt} \quad (1),$$

where *I(t)* is the luminescence intensity and *t* the time.

2.3 Calculation

According to the Judd-Ofelt theory, every radiative $^{S}L_{J} \rightarrow {}^{S'}L'_{J'}$ transition rate in lanthanides can be expressed as in Eq. (2):[34]

$$A_{J-J'} = \frac{64\pi^4 \upsilon^3}{3h(2J+1)} (\chi_{ED} D_{ED} + \chi_{MD} D_{MD}) \quad (2),$$

where υ is the transition barycenter energy, χ_{ED}, χ_{MD} are the local field corrections equal to $n(n^2 + 2)^2/9$ and n^3, respectively, n being the refractive index (**Fig. 1e**), and $D_{ED/MD}$ are electric and magnetic dipole strengths expressed as in Eq. (3) and (4):[34]

$$D_{ED} = e^2 \sum_{\lambda=2,4,6} \Omega_\lambda \left| \langle 4f^N SLJ \| U^\lambda \| 4f^N S'L'J' \rangle \right|^2 \quad (3)$$

$$D_{MD} = \frac{e^2 \hbar^2}{4m^2 c^2} |\langle 4f^N SLJ \| (L + g_s S)^1 \| 4f^N S'L'J' \rangle|^2 \quad (4),$$

where Ω_λ are the J-O parameters characteristic for the host and the matrix parameters are tabulated for each $^{S}L_{J} \rightarrow {}^{S'}L'_{J'}$ transition for each lanthanide ion.

In the case of Eu^{3+}, the $A_{0\text{-}1}$ can be estimated from Eq. (5):[35]

$$A_{0-1} = n^3 (A_{0-1})_{vac} \quad (5),$$

where $(A_{0\text{-}1})_{vac}$ is equal to 14.64 s^{-1}.

The transition rates $A_{0\text{-}J}$ can be calculated from the intensity ratios between the $^5D_0 \rightarrow {}^7F_J$ and the $^5D_0 \rightarrow {}^7F_1$ emission transitions (I_{0J} and I_{01}, respectively) according to Eq. (6):[36]

$$A_{0-J} = A_{0-1} \frac{I_{0J}}{I_{01}} \quad (6)$$

The values of Ω_λ can be calculated from the ratio of integrated intensity of Eu^{3+} emission lines and Eq. (2), (3), (5), (6) and the nonzero reduced matrix parameters $\langle U^\lambda \rangle$ equal to 0.0032, 0.0023 and 0.0002 for λ = 2, 4 and 6, respectively.[37]

The radiative decay time (τ_r) can be calculated from Eq. (7):[38]

$$\tau_r = \frac{1}{A_{tot}} \quad (7),$$

where A_{tot} is given by Eq. (8):

$$A_{tot} = \sum_{J=1,2,4,6} A_{0-J} \quad (8)$$

The non-radiative transition rate is given by Eq. (9) as a difference between the inverse of the experimentally measured and radiative lifetime.

$$W_{non} = \frac{1}{\tau_{exp}} - \frac{1}{\tau_r} \quad (9)$$

The fluorescence intensity ratio (FIR) is given by Eq. (10):[1]

$$FIR = \frac{I_{0-1}}{I_{1-1}} = B \exp\left(-\frac{\Delta E}{kT}\right) \quad (10),$$

where $I_{0\text{-}1}$ and $I_{1\text{-}1}$ are intensities of luminescence originating from $^5D_0 \rightarrow {}^7F_1$ (592 nm) and $^5D_1 \rightarrow {}^7F_1$ (535 nm) transitions, respectively. ΔE is the energy gap between those levels and is equal to 1755 cm^{-1}, k is the Boltzmann's constant and T denotes the temperature. B is an empirical parameter.

The absolute and relative sensitivities of the luminescent thermometer are given by Eq. (11) and (12), respectively:[1]

$$S_a(T) = \left|\frac{\partial}{\partial T} FIR(T)\right| \quad (11)$$

$$S_r(T) = \frac{\left|\frac{\partial}{\partial T} FIR(T)\right|}{FIR\ (T)} = \frac{\Delta E}{kT^2} \quad (12)$$

The theoretical values of B from Eq. (10), denoted as B_{th}, were obtained from Eq. (13):[31]

$$B_{th} = \left(\frac{\upsilon_H}{\upsilon_L}\right)^3 \frac{{\chi_{ED}}^H {D_{ED}}^H + {\chi_{MD}}^H {D_{MD}}^H}{{\chi_{ED}}^L {D_{ED}}^L + {\chi_{MD}}^L {D_{MD}}^L} \quad (13)$$

where indices H and L denote transitions from the higher- and lower-lying levels: $^5D_1$ and $^5D_0$ (same as for Eq. (10)). In the studied case of Eu^{3+}, the components of Eq. (13) are equal to:

$${\chi_{ED}}^H {D_{ED}}^H + {\chi_{MD}}^H {D_{MD}}^H = \eta \cdot 0.0026\Omega_2 \quad (14),$$

where $\eta = e^2\chi_{ED}$, and:

$${\chi_{ED}}^L {D_{ED}}^L + {\chi_{MD}}^L {D_{MD}}^L = n^3 \cdot 9.6 \cdot 10^{-42} \quad (15)$$

The value of absolute sensitivity can be calculated theoretically using Eq. (16):

$$S_a^{th}(T) = \frac{\Delta E}{kT} \cdot B_{th} \exp\left(-\frac{\Delta E}{kT}\right) \quad (16)$$

To calculate the impact of Ω_2 and refractive index n on the value of B, necessary simplifications are made. η is simplified to $e^2n^3(n^2+4)/9$, then B_{th} can be simplified as in Eq. (17):

$$B_{th} \sim \frac{e^2 n^3 (n^2+4) \cdot 2.6 \cdot 10^{-3} \Omega_2}{9 \cdot 9.6 \cdot 10^{-42} n^3} \sim C \cdot (n^2 + 4) \cdot \Omega_2 \quad (17),$$

where C is a constant of order of magnitude 10^{-19}. Then the derivatives of B with respect to n and Ω_2 can be expressed by Eq. (18) and (19):

$$\frac{dB_{th}}{dn} = 2C\Omega_2 n \approx 10^{-39} \quad (18)$$

$$\frac{dB_{th}}{d\Omega_2} = C(n^2 + 4) \approx 10^{-19} \quad (19)$$

3. Results and discussion

The absolute sensitivity (S_a^{th}) of a luminescent thermometer can be estimated from the J-O parameters and the refractive index of the glasses (Eq. (13)-(16)).[31] The excitation and emission spectra (**Fig. 1a**)are characteristic for the Eu^{3+} in a low symmetry environment, as expected for an amorphous solid host.[39] The maximum of luminescence intensity is located

at 612 nm and is assigned to the $^5D_0 \rightarrow {}^7F_2$ electric-dipole (ED) type hypersensitive transition. The J-O parameters are calculated from the intensity of Eu^{3+} emission from the $^5D_0$ level (570 – 850 nm) (**Fig. 1b,c,d**),[40] and from the refractive index of the glasses which increases with the addition of SiO_2 or B_2O_3 (**Table 1, Fig. 1e**). From the J-O parameters (**Table 1**), the absolute sensitivity (S_a^{th}) is expected to increase with the addition of SiO_2 or B_2O_3 in the same matter, from 0.0243% K^{-1} to 0.0256% K^{-1} at 473 K (**Table 1**).

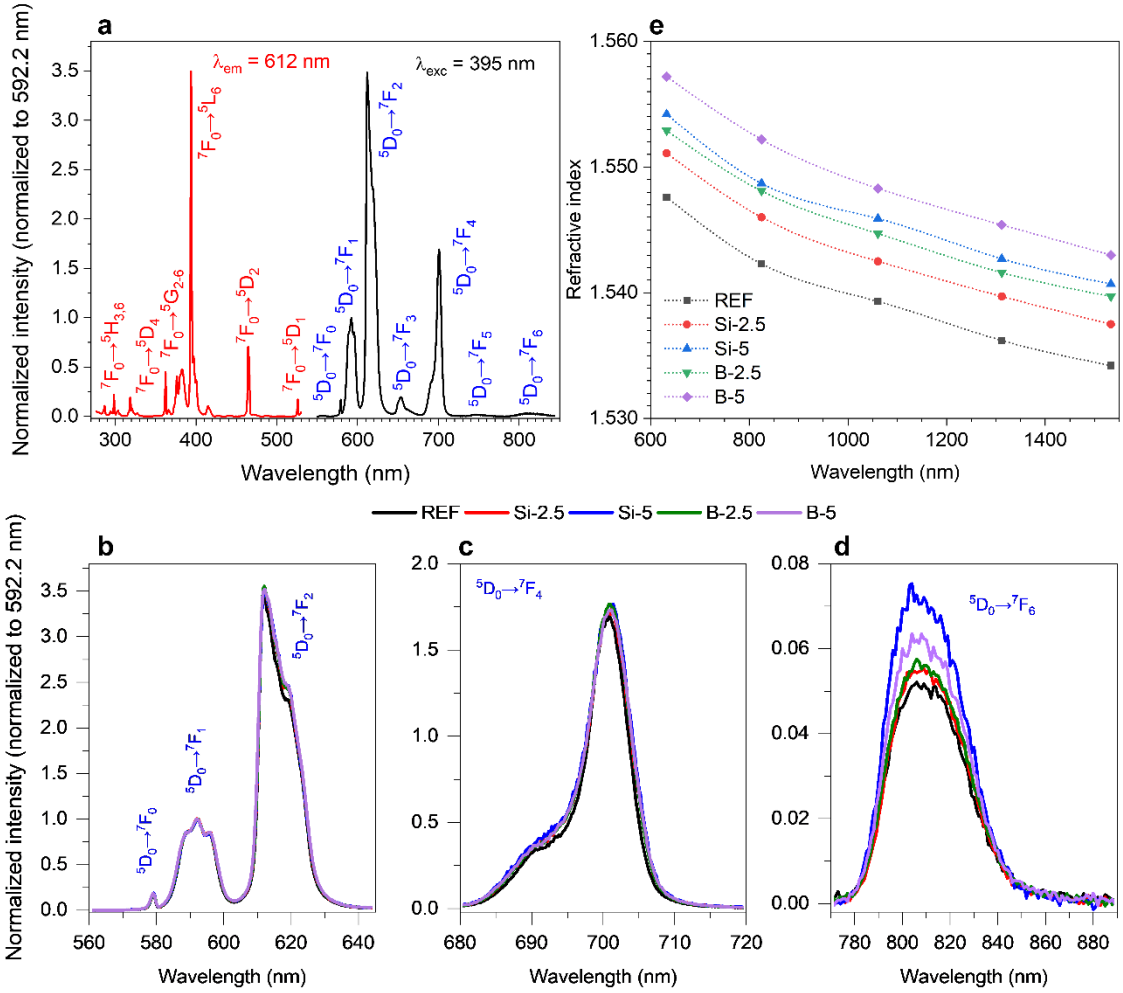

Fig. 1. (a) Excitation (red) and emission (black) spectra of the reference sample ($x = 0$). The monitored wavelength for excitation is 612 nm and the excitation wavelength for emission is 395 nm. (b,c,d) Emission spectra of the Eu^{3+}-doped glasses in selected regions for $^5D_0 \rightarrow {}^7F_J$ transitions: J = 0, 1, 2 (b), J = 4 (c) and J = 6 (d) normalized to the intensity of $^5D_0 \rightarrow {}^7F_1$

transition. The excitation wavelength for emission is 395 nm. (e) Refractive index measured for the five different bulk glass samples.

To test the reliability of the above calculations, the absolute thermometric sensitivity of studied materials was determined experimentally (S_a^{exp}). The emission spectra of the Eu^{3+}-doped samples were measured from 77 to 773 K (**Fig. 2a**). Here, the transitions $^5D_0 \rightarrow {}^7F_J$, where J = 0,…,4, are located at 580 – 750 nm spectral region and their intensity is steady up to 273 K and then drops as a result of thermal quenching whereas the intensity of transitions $^5D_1 \rightarrow {}^7F_J$, where J = 0,1,2 located at 520 – 560 nm spectral region increases for temperatures above 273 K up to a certain quenching temperature (T_q) (**Fig. 2b,c**). The drop in the emission intensity from the $^5D_1$ level for temperatures above T_q is due to the depopulation through the $^5D_1$ level crossing over with the ground state parabola in a single coordinate diagram.[41] With addition of SiO_2 or B_2O_3, T_q shifts from 623 K to higher temperatures (**Table 2**) in agreement with the thermal properties of the glasses: as shown in **Table 3**, the T_g, T_x and T_p increase with the addition of SiO_2 or B_2O_3, as observed by others for various glass systems.[42,43]

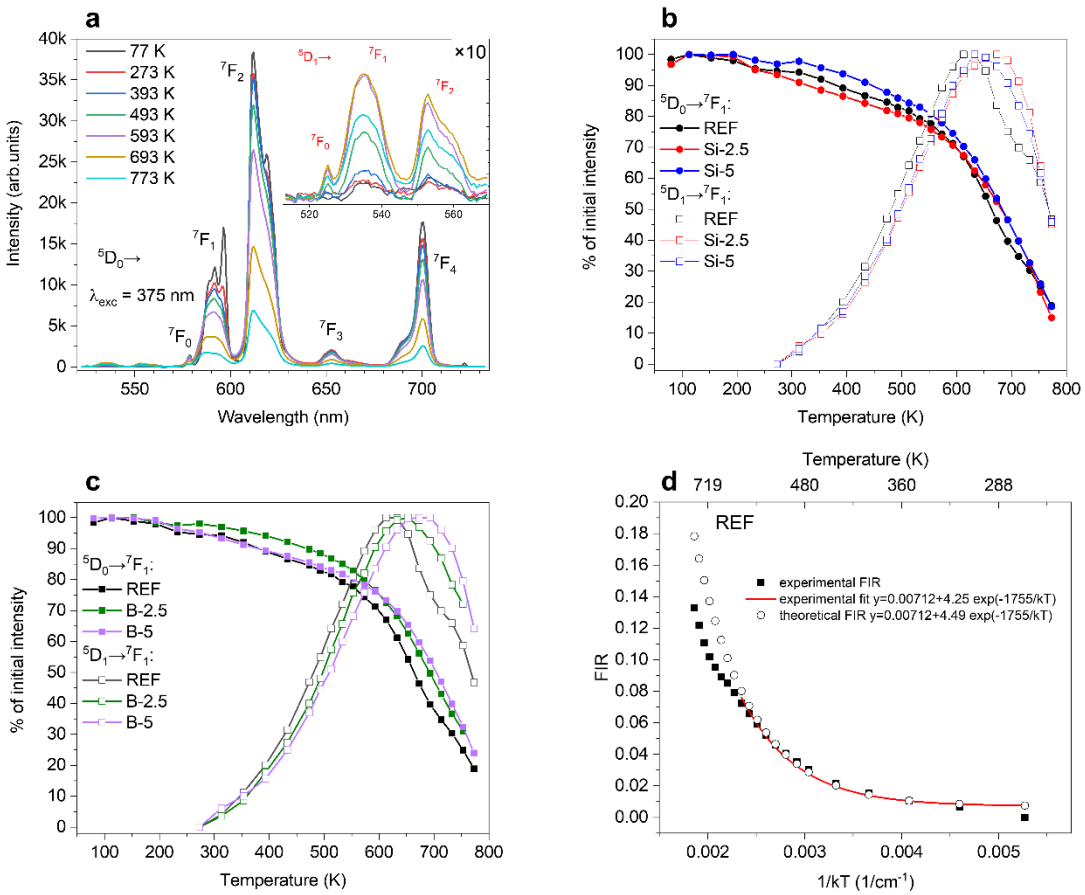

Fig. 2. (a) Thermally dependent Eu^{3+} emission spectra of REF glass excited at 375 nm. (b,c) Luminescence intensity of the transitions from $^5D_0$ and $^5D_1$ levels to $^7F_1$ level for REF, Si-2.5, Si-5 samples (b) and REF, B-2.5, B-5 samples (c) as a function of temperature. (d) Theoretical and experimental FIR for the REF glass, taken as an example.

Fig. 2d depicts the experimentally measured FIR and the theoretical FIR determined from the J-O parameters (Eq. (10) and (13)), clearly showing the agreement between those values for temperatures under T_q. Since the occupation of both $^5D_0$ and $^5D_1$ levels is governed by the Boltzmann law [44] and the emission intensity originating from an excited energy level is proportional to its population, the FIR can be fitted with Eq. (10). The absolute thermometric sensitivities (S_a^{exp}) of the glasses at 473 K are listed in **Table 1** and they are in good agreement

with those obtained theoretically. S_a^{exp} increases with addition of SiO_2 or B_2O_3 as expected from the J-O theory. B and Si have similar impact on S_a^{exp}; the increase in S_a^{exp} when adding 2.5 mol% B_2O_3 is similar to that of adding 5 mol% of SiO_2. The relative sensitivity S_r, estimated from the S_a^{exp}, remains independent of the glass composition withing the limit of measurement uncertainty and is equal to ~(0.9 ± 0.2)% K^{-1} (at T = 473 K), which is similar to the 1.68% K^{-1} reported at 288 K for $[60(NaPO_3)_3 + 35Al(PO_3)_3] + 5Eu_2O_3$ glass by Morassuti *et al.*[15] It is worthwhile highlighting that the relative sensitivity reported by Morassuti *et al.* was measured in different thermometric mode, using $^7F_0$ and $^7F_1$ as thermally coupled levels, thus a direct comparison cannot be made.

According to the theory, the absolute sensitivity depends on the Ω_2 parameter and on the refractive index which increases as *x* increases (**Fig. 1e**). As shown in **Table 1**, the Ω_2 and Ω_4 parameters of the glasses are independent of the glass composition indicating that the site of Eu^{3+} does not change when adding SiO_2 or B_2O_3 in the glasses, which is in agreement with their spectroscopic properties. As highlighted in **Fig. 1b**, the addition of SiO_2 or B_2O_3 has no noticeable effect on the shape and position of the $^5D_0 \rightarrow {}^7F_0$ transition peak confirming that the changes in the glass composition have no significant impact on the site of Eu^{3+}. Thus, Si and B are not expected to be in the coordination sites of Eu^{3+} ions. However, the changes in the glass composition have an impact on the intensity of the emissions in the 550-900 nm range which increases with the addition of SiO_2 and B_2O_3, the impact being stronger for the addition of B_2O_3 (**Fig. 3a,b**), indicating that the structural units around the Eu^{3+} change. The above result correlates with the increase in the luminescence QY (**Table 2**): QY increases drastically reaching almost 100% for samples prepared with B_2O_3. Such high value of QY is not uncommon in glass and glass-ceramic materials,[45–47] e.g. QY between 64 and 99% was observed for Yb^{3+}-doped oxyfluoride glass-ceramics,[46] and results from a low rate of non-radiative processes according to Malashkevich *et al.*[45] Similar low rate of non-radiative transition W_{non} was observed for studied samples (Table 2). One can notice that the Ω_6 parameter

increases from $6.7 \cdot 10^{-20}$ to $9.1 \cdot 10^{-20}$ cm^2 when adding 5 mol% of SiO_2 and to $7.8 \cdot 10^{-20}$ cm^2 when adding 5 mol% of B_2O_3 (**Table 1**). This increase in Ω_6 can be attributed to an increase in the π-electron donation from the phosphate groups in agreement with Ebendorff-Heidepriem *et al.*[26] Different studies on phosphate glasses related the Ω_6 as an indicator of high host rigidity.[48] Thus, the significant changes in the Ω_6 parameter values might suggest that the addition of SiO_2 or B_2O_3 increases the rigidity of the network.[49] The increase in Ω_6 parameter is larger from the SiO_2 containing glasses compared to B_2O_3 containing glasses indicating that the network of the SiO_2 containing glasses has higher connectivity probably due to the covalent Si-O bonds. The value of Ω_6 for the Si-5 sample seems to be higher than reported for most Eu^{3+} - doped glass systems but still within expected range [50].Similar increase in Ω_6 with little observed changes in Ω_2 and Ω_4 has been reported for other glasses and has been linked to the ionic packing ratio of the glass host.[51] One can notice that the J-O parameters of the investigated glasses follow the $\Omega_6 > \Omega_2 > \Omega_4$ trend, in line with that reported for other phosphate glasses [52]and different than trends reported for other glass systems [53].

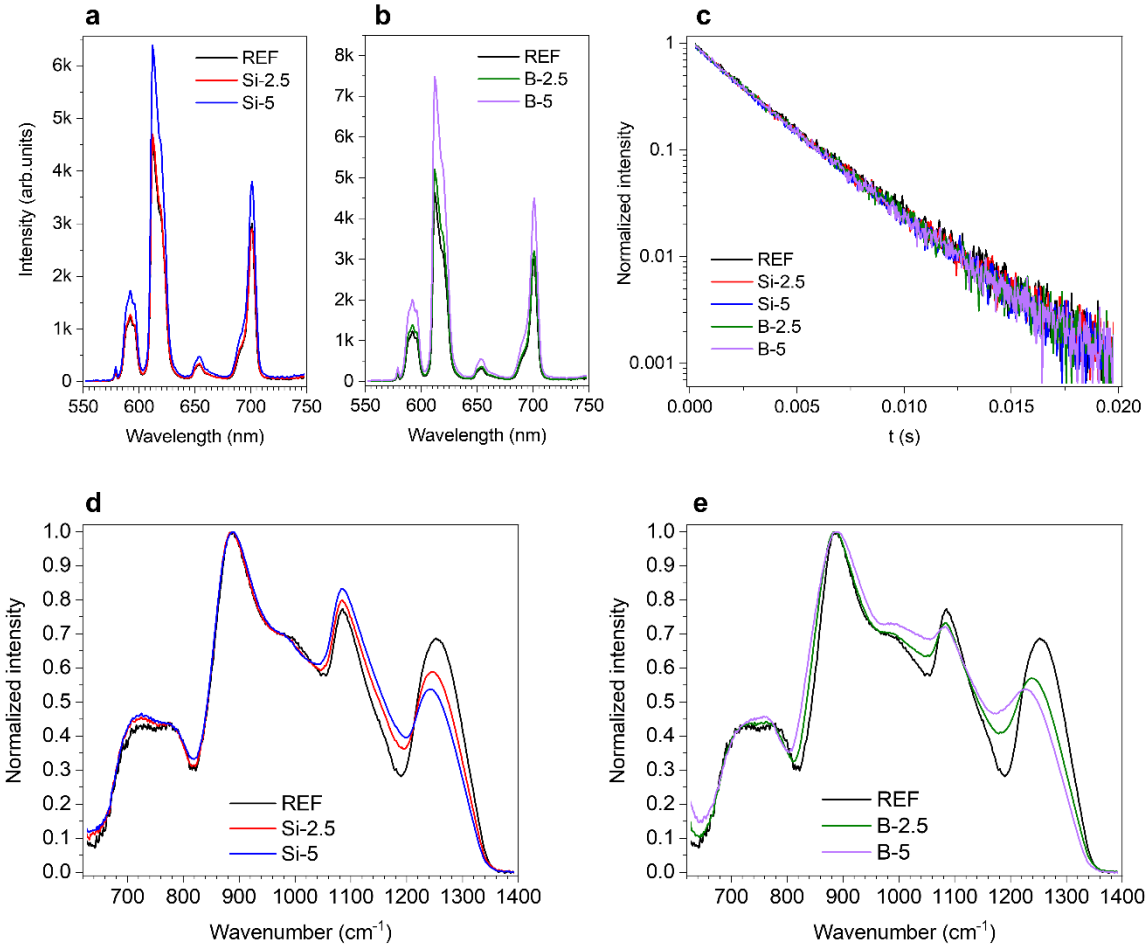

Fig. 3. (A,B) Luminescence intensity of the samples with addition of SiO_2 (a) and B_2O_3 (b) in relation to the REF sample. The excitation is at 395 nm. (c) Luminescence decay curves of the Eu^{3+}-doped glasses excited at 395 nm and monitored at 612 nm. (d,e) Normalized IR spectra of the glasses with varying SiO_2 (d) and B_2O_3 concentration (e).

The J-O parameters have been used to estimate the radiative decay time (τ_r) (Eq. (7)). The experimental decay time (τ_{exp}) were measured (**Fig. 3c**) and are listed in **Table 2**. They are in agreement with τ_r. They are characteristic for the Eu^{3+} ions in a low-symmetry environment and are similar to those reported in a previous study.[15] As the radiative decay time decreases with increasing the concentration of SiO_2 or B_2O_3 as a result of the increased refractive index (**Fig. 1e**), the experimental decay time is expected to decrease as well. One can notice that the values

of τ_{exp} and τ_r get more similar while increasing the concentration of SiO_2 or B_2O_3, which corresponds to a decrease in the non-radiative transitions rate (W_{non}) (**Table 2**). The above result agrees with the increase in QY as *x* increases, since the closer the decay time is to the radiative decay time, the less contribution comes from the non-radiative transitions, resulting in a higher phosphor efficiency.

As the Ω_2 parameter remains unchanged when adding SiO_2 or B_2O_3, the increase of the absolute sensitivity results mainly from the increase in the refractive index. Therefore, it is crucial to understand the impact of B_2O_3 or SiO_2 on the refractive index of the phosphate glass and so on the structure of the glasses, which can be studied and confirmed by means of differential thermal analysis and IR spectroscopy. The molar volume of the glass decreased with the addition of SiO_2 or B_2O_3 (**Table 3**), which indicates a closer packing of coordination polyhedral as *x* increases[54] and gives indication that the addition of SiO_2 or B_2O_3 increased the rigidity of the glass as confirmed from the thermal properties reported in **Table 3**. The T_g, T_x and T_p increased with the addition of SiO_2 or B_2O_3 (**Table 3**), as observed by others for various glass systems,[42,43,54] and the increase in T_g is larger when adding B_2O_3 than when adding SiO_2.

To gain insight on the structural changes induced by the addition of SiO_2 or B_2O_3, one must study the changes in structural units by means of IR spectroscopy. IR bands were observed in the IR spectra along the range 620 - 1400 cm^{-1} (**Fig. 3d,e**) located at around 700-800, 880, 975, 1080, 1130 and 1250 cm^{-1}. Similar IR spectra were reported by Massera et al.[29] The bands at 700-800 cm^{-1} result from the symmetric vibration of the P-O-P groups of the Q_2 units.[55] The most intense band at 880 cm^{-1} is associated to the asymmetric vibration of the same unit.[56–58] The band located at 975 cm^{-1} originates from the symmetric vibrations of the PO_3^{2-} groups of the Q_1 units, whereas the band at 1250 cm^{-1} can be assigned to the asymmetric vibrations of the PO_2 groups of the Q_2 units. The bands at 1080 and 1190 cm^{-1} can be related to both Q_1 and Q_2 units. Finally, the shoulders at ~850, 960 and 1020 cm^{-1} can be associated to the asymmetric stretching vibration of Q_2 units in chains, small and large rings, respectively.[56,59]

A decrease in intensity of the band at 1250 cm^{-1} associated with an increase in intensity of the band at 1080 cm^{-1} in the IR spectra of the Si containing glasses can be observed, indicating the disruption of the PO_2 asymmetric Q_2 vibration mode with the creation of P-O-Si bonds at the expense of P-O-P bonds.[60] The formation of P-O-Si bonds when adding SiO_2 in phosphate glass has been reported by Glorieux *et al.*[61] Ahmadi Mooghari *et al.* interpreted the extinction of the band at 1250 cm^{-1} and the simultaneous appearance of the band at 1120 cm^{-1} as the possible mode of asymmetrical bond stretching vibrations of the Si–O (oxygen bridges between the [SiO_4] tetrahedra) in Si–O–Si.[62,63] It has been shown that in glasses in the Na_2O–SiO_2–P_2O_5 system, SiO_2 and P_2O_5 form a silica–phosphate network when the content of Na_2O is lower than P_2O_5[64] as in the case of the studied glasses. Hence the addition of SiO_2 is confirmed to provide the interlinkage between the ions increasing the rigidity of the structure. With the addition of B_2O_3 (**Fig. 3e**), the full width at half maximum (FWHM) of the most intense band at 880 cm^{-1} increases, which is associated with the longer bridging angles and distances.[65] While the P-O-B bonds cannot be directly observed in the IR spectra, due to the overlapping bands, they can be inferred from the decrease of the bands associated with the P-O-P bonds and from the increase in T_g.[29] While Q^1 units are expected to form at the expense of Q^2 units in the Si and B containing glasses, a larger number of rings are expected to form when adding B_2O_3 as suggested by the large intensity of the shoulder at ~1020 cm^{-1}. The shoulder at 1020 cm^{-1} can also be related to the B-O stretching mode of the BO_4 group. The depolymerization of the phosphate network due to the incorporation of BO_4 and BO_3 structural units is also evidenced by the shift to lower wavenumber of the band at 1250 cm^{-1}.[29,54] It is the depolymerization of the phosphate networks associated with the increase in Q^1 units at the expense of the Q^2 units, which leads to the increase of n. The formation of new bonds with Si and B ions at the expense of P-O-P bonds is thought to enhance the rigidity of the structure, increasing the Ω_6 parameter. To summarize, all these structural changes result in an

enhancement of the thermometric sensitivity although Si and B have no noticeable impact on the site of Eu^{3+} ions.

It is clearly shown here that there are two types of limitations connected with this theoretical approach. First is the limitation of the quantitative assessment of the changes in absolute sensitivity: while the model correctly predicts the enhancement of the said value when modifying the glass composition, it does not correctly predict the magnitude of enhancement when adding larger amount of B_2O_3. As already mentioned, the absolute sensitivity is calculated from n and Ω_2. Given that the changes in n and in Ω_2 when increasing x are of magnitude 10^{-2} and 10^{-21}, respectively, so based on Eq. (19) and (19) the impact of the change in n on the estimation of the absolute sensitivity is one order of magnitude weaker than the one in Ω_2. The site of Eu^{3+} ions needs to change significantly for the model to predict the change in the absolute sensitivity. The model does not take into account the changes in the connectivity of the glass network when modifying the glass composition. The second limitation stems from the fact that the model does not take into account other levels than the coupled pair $^5D_0$ and $^5D_1$. Therefore, the depopulation of the $^5D_1$ level by thermal quenching cannot be modeled using this method. Hence, the method only works up to T_q. It is apparent for the FIR, when the experimental and theoretical values deviate for $1/kT_q = 0.0023$, which correspond to $T_q = 623$ K (**Fig. 2d**).

4. Conclusion

The applicability of the Judd-Ofelt theory for predicting the thermometric performance of the glass luminescent material based solely on the Judd-Ofelt parameters was demonstrated on glass materials. The J-O parameters were used to predict the thermometric performance of phosphate glasses which was validated with experimental data. The absolute thermometric sensitivity was found to depend on the structure of the glass. Indeed, the addition of SiO_2 or B_2O_3 disrupts the phosphate network with the creation of P-O-Si/B bonds at the expense of P-

O-P increasing the rigidity of the structure and the refractive index and so the absolute sensitivity.

The applicability of the Judd-Ofelt theory for predicting the thermometric parameters of a glass luminescent material is clearly demonstrated in this paper and allows for further development of novel efficient luminescent thermal sensors with high sensitivity without measuring systematically the glasses spectroscopic properties as a function of temperature. In this study, only a very narrow range of variation was covered and so the continuous changes of the thermometric sensitivity are small. Nonetheless, we demonstrated a great potential of the theory to predict the thermometric sensitivity of new materials.

Acknowledgements

B. B. would like to acknowledge the Polish National Agency for Academic Exchange under the Bekker Programme, project PPN/BEK/2020/1/00074 and L. P. the Academy of Finland (Flagship Programme, Photonics Research and Innovation PREIN-320165 and Academy Project -326418).

Conflict of Interest

The authors declare no conflict of interest.

Author Contributions

B. B. and L. P. conceived the idea and designed the research. B. B., C. N., D. P. and T. H. Q. V. performed the experiments. B. B and L. P. analyzed and interpreted the results. B. B. drafted the manuscript, L. P. and P. J. D. supervised the project, and all authors contributed to the writing of the manuscript.

References

[1] C.D.S. Brites, A. Millán, L.D. Carlos, Lanthanides in Luminescent Thermometry, in: Handb. Phys. Chem. Rare Earths, Elsevier, 2016: pp. 339–427. https://doi.org/10.1016/bs.hpcre.2016.03.005.

[2] Y. Zhao, X. Wang, Y. Zhang, Y. Li, X. Yao, Winning wide-temperature-range and high-sensitive thermometry by a multichannel strategy of dual-lanthanides in the new tungstate phosphors, J. Alloys Compd. 834 (2020) 154998. https://doi.org/10.1016/j.jallcom.2020.154998.

[3] D. Stefańska, B. Bondzior, T.H.Q. Vu, M. Grodzicki, P.J. Dereń, Temperature sensitivity modulation through changing the vanadium concentration in a $La_2MgTiO_6:V^{5+}$, Cr^{3+} double perovskite optical thermometer, Dalt. Trans. 50 (2021) 9851–9857. https://doi.org/10.1039/D1DT00911G.

[4] F. Qian, J. Zhang, Various strategies for optical thermometry with high sensitivities based on rare earth ions doped $BaY_2Si_3O_{10}$ phosphors, Mater. Res. Bull. 122 (2020) 110660. https://doi.org/10.1016/j.materresbull.2019.110660.

[5] T.H.Q. Vu, B. Bondzior, D. Stefańska, P.J. Dereń, Exploration of the Temperature Sensing Ability of $La_2MgTiO_6:Er^{3+}$ Double Perovskites Using Thermally Coupled and Uncoupled Energy Levels, Mater. 2021, Vol. 14, Page 5557. 14 (2021) 5557. https://doi.org/10.3390/MA14195557.

[6] K. Elzbieciak-Piecka, C. Matuszewska, L. Marciniak, Step by step designing of sensitive luminescent nanothermometers based on Cr^{3+},Nd^{3+} co-doped $La_{3-x}Lu_xAl_{5-y}Ga_yO_{12}$ nanocrystals, New J. Chem. 43 (2019) 12614–12622. https://doi.org/10.1039/C9NJ03167G.

[7] D. Stefańska, B. Bondzior, T.H.Q. Vu, N. Miniajluk-Gaweł, P.J. Dereń, The influence of morphology and Eu^{3+} concentration on luminescence and temperature sensing behavior of Ba_2MgWO_6 double perovskite as a potential optical thermometer, J. Alloys Compd. 842 (2020) 155742. https://doi.org/10.1016/j.jallcom.2020.155742.

[8] C.D.S. Brites, P.P. Lima, N.J.O. Silva, A. Millán, V.S. Amaral, F. Palacio, L.D. Carlos, Thermometry at the nanoscale, Nanoscale. 4 (2012) 4799. https://doi.org/10.1039/c2nr30663h.

[9] O.A. Savchuk, J.J. Carvajal, M.C. Pujol, E.W. Barrera, J. Massons, M. Aguilo, F. Diaz, Ho,Yb:$KLu(WO_4)_2$ Nanoparticles: A Versatile Material for Multiple Thermal Sensing Purposes by Luminescent Thermometry, J. Phys. Chem. C. 119 (2015) 18546–18558. https://doi.org/10.1021/ACS.JPCC.5B03766.

[10] A. Tymiński, E. Śmiechowicz, I.R. Martín, T. Grzyb, Ultraviolet- A nd Near-Infrared-Excitable $LaPO_4:Yb^{3+}/Tm^{3+}/Ln^{3+}$(Ln = Eu, Tb) Nanoparticles for Luminescent Fibers and Optical Thermometers, ACS Appl. Nano Mater. 3 (2020) 6541–6551. https://doi.org/10.1021/acsanm.0c01025.

[11] A.M. Kaczmarek, M. Suta, H. Rijckaert, T.P. van Swieten, I. Van Driessche, M.K. Kaczmarek, A. Meijerink, High temperature (nano)thermometers based on $LiLuF_4:Er^{3+},Yb^{3+}$ nano- and microcrystals. Confounded results for core–shell nanocrystals, J. Mater. Chem. C. 9 (2021) 3589–3600. https://doi.org/10.1039/D0TC05865C.

[12] L.T.K. Giang, K. Trejgis, L. Marciniak, N. Vu, L.Q. Minh, Fabrication and characterization of up-converting β-$NaYF_4:Er^{3+},Yb^{3+}$@$NaYF_4$ core–shell nanoparticles for temperature sensing applications, Sci. Rep. 10 (2020). https://doi.org/10.1038/S41598-020-71606-6.

[13] K.M. McCabe, E.J. Lacherndo, I. Albino-Flores, E. Sheehan, M. Hernandez, LacI(Ts)-Regulated Expression as an In Situ Intracellular Biomolecular Thermometer, Appl. Environ. Microbiol. 77 (2011) 2863. https://doi.org/10.1128/AEM.01915-10.

[14] V. Lojpur, M. Nikolic, L. Mancic, O. Milosevic, M.D. Dramicanin, Y_2O_3:Yb,Tm and Y_2O_3:Yb,Ho powders for low-temperature thermometry based on up-conversion fluorescence, Ceram. Int. 39 (2013) 1129–1134. https://doi.org/10.1016/J.CERAMINT.2012.07.036.

[15] C.Y. Morassuti, L.A.O. Nunes, S.M. Lima, L.H.C. Andrade, Eu^{3+}- doped alumino-phosphate glass for ratiometric thermometer based on the excited state absorption, J. Lumin. 193 (2018) 39–43. https://doi.org/10.1016/J.JLUMIN.2017.09.001.

[16] D. Huang, Q. Ouyang, B. Liu, B. Chen, Y. Wang, C. Yuan, H. Xiao, H. Lian, J. Lin, Mn^{2+}/Mn^{4+} co-doped $LaM_{1-x}Al_{11-y}O_{19}$ (M = Mg, Zn) luminescent materials: electronic structure, energy transfer and optical thermometric properties, Dalt. Trans. 50 (2021) 4651–4662. https://doi.org/10.1039/D1DT00153A.

[17] L. Zhou, L. Zhou, P. Du, P. Du, W. Li, W. Li, L. Luo, L. Luo, G. Xing, G. Xing, Composition Regulation Triggered Multicolor Emissions in Eu^{2+}-Activated $Li_4(Sr_{1-x}Ca_{1+x})(SiO_4)_2$ for a Highly Sensitive Thermometer, Ind. Eng. Chem. Res. 59 (2020) 9989–9996. https://doi.org/10.1021/ACS.IECR.0C00967/SUPPL_FILE/IE0C00967_SI_001.PDF.

[18] S. Gharouel, L. Marciniak, A. Lukowiak, W. Strek, K. Horchani-Naifer, M. Férid, Impact of grain size, Pr^{3+} concentration and host composition on non-contact

temperature sensing abilities of polyphosphate nano- and microcrystals, J. Rare Earths. 37 (2019) 812–818. https://doi.org/10.1016/J.JRE.2018.12.001.

[19] W. Xu, X. Zhu, D. Zhao, L. Zheng, F. Shang, Z. Zhang, Optical thermometry based on near-infrared luminescence from phosphors mixture, J. Rare Earths. (2020). https://doi.org/10.1016/J.JRE.2020.12.011.

[20] K. Maciejewska, A. Bednarkiewicz, A. Meijerink, L. Marciniak, Correlation between the Covalency and the Thermometric Properties of Yb^{3+} /Er^{3+} Codoped Nanocrystalline Orthophosphates, J. Phys. Chem. C. 125 (2021) 2659–2665. https://doi.org/10.1021/acs.jpcc.0c09532.

[21] J. Drabik, R. Lisiecki, L. Marciniak, Optimization of the thermometric performance of single band ratiometric luminescent thermometer based on Tb^{3+} luminescence by the enhancement of thermal quenching of GSA-excited luminescence in TZPN glass, J. Alloys Compd. 858 (2021) 157690. https://doi.org/10.1016/j.jallcom.2020.157690.

[22] L. Wortmann, S. Suyari, T. Ube, M. Kamimura, K. Soga, Tuning the thermal sensitivity of β-$NaYF_4$: Yb^{3+}, Ho^{3+}, Er^{3+} nanothermometers for optimal temperature sensing in OTN-NIR (NIR II/III) biological window, J. Lumin. 198 (2018) 236–242. https://doi.org/10.1016/J.JLUMIN.2018.01.049.

[23] W. Piotrowski, K. Kniec, L. Marciniak, Enhancement of the Ln^{3+} ratiometric nanothermometers by sensitization with transition metal ions, J. Alloys Compd. 870 (2021). https://doi.org/10.1016/J.JALLCOM.2021.159386.

[24] R.T. Moura, A.N. Carneiro Neto, R.L. Longo, O.L. Malta, On the calculation and interpretation of covalency in the intensity parameters of *4f–4f* transitions in Eu^{3+} complexes based on the chemical bond overlap polarizability, J. Lumin. 170 (2016) 420–430. https://doi.org/10.1016/J.JLUMIN.2015.08.016.

[25] S. Tanabe, T. Ohyagi, N. Soga, T. Hanada, Compositional dependence of Judd-Ofelt parameters of Er^{3+} ions in alkali-metal borate glasses, Phys. Rev. B. 46 (1992) 3305–3310. https://doi.org/10.1103/PhysRevB.46.3305.

[26] H. Ebendorff-Heidepriem, D. Ehrt, M. Bettinelli, A. Speghini, Effect of glass composition on Judd–Ofelt parameters and radiative decay rates of Er^{3+} in fluoride phosphate and phosphate glasses, J. Non. Cryst. Solids. 240 (1998) 66–78. https://doi.org/10.1016/S0022-3093(98)00706-6.

[27] P. Goldner, F. Auzel, Application of standard and modified Judd-Ofelt theories to a praseodymium-doped fluorozirconate glass, J. Appl. Phys. 79 (1996) 7972–7977. https://doi.org/10.1063/1.362347.

[28] P. Babu, C.K. Jayasankar, Optical spectroscopy of Eu^{3+} ions in lithium borate and lithium fluoroborate glasses, Phys. B Condens. Matter. 279 (2000) 262–281. https://doi.org/10.1016/S0921-4526(99)00876-5.

[29] J. Massera, Y. Shpotyuk, F. Sabatier, T. Jouan, C. Boussard-Plédel, C. Roiland, B. Bureau, L. Petit, N.G. Boetti, D. Milanese, L. Hupa, Processing and characterization of novel borophosphate glasses and fibers for medical applications, J. Non. Cryst. Solids. 425 (2015) 52–60. https://doi.org/10.1016/j.jnoncrysol.2015.05.028.

[30] J. Massera, L. Petit, T. Cardinal, J.J. Videau, M. Hupa, L. Hupa, Thermal properties and surface reactivity in simulated body fluid of new strontium ion-containing phosphate glasses, J. Mater. Sci. Mater. Med. 24 (2013) 1407–1416. https://doi.org/10.1007/s10856-013-4910-9.

[31] A. Ćirić, S. Stojadinović, M.D. Dramićanin, An extension of the Judd-Ofelt theory to the field of lanthanide thermometry, J. Lumin. 216 (2019) 116749. https://doi.org/10.1016/j.jlumin.2019.116749.

[32] I.E. Kolesnikov, D. V. Mamonova, M.A. Kurochkin, E.Y. Kolesnikov, E. Lähderanta, Eu^{3+}-doped ratiometric optical thermometers: Experiment and Judd-Ofelt modelling, Opt. Mater. (Amst). 112 (2021) 110797. https://doi.org/10.1016/j.optmat.2020.110797.

[33] R. Lisiecki, J. Komar, B. Macalik, M. Glowacki, M. Berkowski, W. Ryba-Romanowski, Exploring the Impact of Structure-Sensitivity Factors on Thermographic Properties of Dy^{3+}-Doped Oxide Crystals, Mater. 2021, Vol. 14, Page 2370. 14 (2021) 2370. https://doi.org/10.3390/MA14092370.

[34] W.T. Carnall, J.P. Hessler, F.W. Wagner, Transition probabilities in the absorption and fluorescence spectra of lanthanides in molten lithium nitrate -potassium nitrate eutectic, J. Phys. Chem. 82 (1978) 2152–2158. https://doi.org/10.1021/j100509a003.

[35] T.S. Sreena, P. Prabhakar Rao, T. Linda Francis, A.K. V. Raj, P.S. Babu, Structural and photoluminescence properties of stannate based displaced pyrochlore-type red phosphors: $Ca_{3-x}Sn_3Nb_2O_{14}$:xEu^{3+}, Dalt. Trans. 44 (2015) 8718–8728. https://doi.org/10.1039/C4DT03800B.

[36] C. De Mello Donegá, S. Alves, G.F. De Sá, Synthesis, luminescence and quantum yields of Eu(III) mixed complexes with 4,4,4-trifluoro-1-phenyl-1,3-butanedione and 1,10-phenanthroline-N-oxide, J. Alloys Compd. 250 (1997) 422–426. https://doi.org/10.1016/S0925-8388(96)02562-5.

[37] W.T. Carnall, P.R. Fields, K. Rajnak, Spectral Intensities of the Trivalent Lanthanides and Actinides in Solution. II. Pm^{3+}, Sm^{3+}, Eu^{3+}, Gd^{3+}, Tb^{3+}, Dy^{3+}, and Ho^{3+}, J. Chem.

Phys. 49 (1968) 4412–4423. https://doi.org/10.1063/1.1669892.

[38] M.J. Weber, Probabilities for Radiative and Nonradiative Decay of Er^{3+} in LaF_3, Phys. Rev. 157 (1967) 262–272. https://doi.org/10.1103/PhysRev.157.262.

[39] K. Binnemans, Interpretation of europium(III) spectra, Coord. Chem. Rev. 295 (2015) 1–45. https://doi.org/10.1016/j.ccr.2015.02.015.

[40] A. Ćirić, Ł. Marciniak, M.D. Dramićanin, Self-referenced method for the Judd–Ofelt parametrisation of the Eu^{3+} excitation spectrum, Sci. Rep. 12 (2022) 563. https://doi.org/10.1038/s41598-021-04651-4.

[41] M.D. Chambers, P.A. Rousseve, D.R. Clarke, Decay pathway and high-temperature luminescence of Eu^{3+} in Ca2Gd8Si6O26, J. Lumin. 129 (2009) 263–269. https://doi.org/10.1016/J.JLUMIN.2008.10.008.

[42] R. Bala, A. Agarwal, S. Sanghi, S. Khasa, Influence of SiO_2 on the structural and dielectric properties of $ZnO{\cdot}Bi_2O_3{\cdot}SiO_2$ glasses, J. Integr. Sci. Technol. 3(1) (2015) 6–13.

[43] J. Massera, C. Claireaux, T. Lehtonen, J. Tuominen, L. Hupa, M. Hupa, Control of the thermal properties of slow bioresorbable glasses by boron addition, J. Non. Cryst. Solids. 357 (2011) 3623–3630. https://doi.org/10.1016/J.JNONCRYSOL.2011.06.037.

[44] V. Lojpur, S. Ćulubrk, M.D. Dramićanin, Ratiometric luminescence thermometry with different combinations of emissions from Eu^{3+} doped $Gd_2Ti_2O_7$ nanoparticles, J. Lumin. 169 (2016) 534–538. https://doi.org/10.1016/j.jlumin.2015.01.027.

[45] G.E. Malashkevich, V.N. Sigaev, N. V. Golubev, V.I. Savinkov, P.D. Sarkisov, I.A. Khodasevich, V.I. Dashkevich, A. V. Mudryi, Luminescence of borogermanate glasses activated by Er^{3+} and Yb^{3+} ions, J. Non. Cryst. Solids. 357 (2011) 67–72. https://doi.org/10.1016/J.JNONCRYSOL.2010.09.007.

[46] J. Thomas, T. Meyneng, Y. Ledemi, A. Rakotonandrasana, D. Seletskiy, L. Maia, Y. Messaddeq, R. Kashyap, Oxyfluoride glass-ceramics: a bright future for laser cooling, in: R.I. Epstein, D. V. Seletskiy, M. Sheik-Bahae (Eds.), Photonic Heat Engines Sci. Appl. II, SPIE, 2020: p. 14. https://doi.org/10.1117/12.2546969.

[47] A. Belykh, L. Glebov, C. Lerminiaux, S. Lunter, M. Mikhailov, A. Plyukhin, M. Prassas, A. Przhevuskii, Spectral and luminescence properties of neodymium in chalcogenide glasses, J. Non. Cryst. Solids. 213–214 (1997) 238–244. https://doi.org/10.1016/S0022-3093(97)00068-9.

[48] N. Chanthima, Y. Tariwong, J. Kaewkhao, N.W. Sangwaranatee, N. Sangwaranatee, Effect of Alkali Oxides on Luminescence Properties of Eu^{3+}-doped Aluminium

Phosphate Glasses, Mater. Today Proc. 17 (2019) 1906–1913. https://doi.org/10.1016/J.MATPR.2019.06.229.

[49] M. Seshadri, M. Radha, D. Rajesh, L.C. Barbosa, C.M.B. Cordeiro, Y.C. Ratnakaram, Effect of ZnO on spectroscopic properties of Sm^{3+} doped zinc phosphate glasses, Phys. B Condens. Matter. 459 (2015) 79–87. https://doi.org/10.1016/j.physb.2014.11.016.

[50] C. Görller-Walrand, K. Binnemans, Chapter 167 Spectral intensities of f-f transitions, in: 1998: pp. 101–264. https://doi.org/10.1016/S0168-1273(98)25006-9.

[51] H. Takebe, Y. Nageno, K. Morinaga, Compositional Dependence of Judd-Ofelt Parameters in Silicate, Borate, and Phosphate Glasses, J. Am. Ceram. Soc. 78 (1995) 1161–1168. https://doi.org/10.1111/j.1151-2916.1995.tb08463.x.

[52] L. Boehm, R. Reisfeld, N. Spector, Optical transitions of Sm3+ in oxide glasses, J. Solid State Chem. 28 (1979) 75–78. https://doi.org/10.1016/0022-4596(79)90060-4.

[53] M. Dejneka, E. Snitzer, R.E. Riman, Blue, green and red fluorescence and energy transfer of Eu^{3+} in fluoride glasses, J. Lumin. 65 (1995) 227–245. https://doi.org/10.1016/0022-2313(95)00073-9.

[54] L. Koudelka, P. Mošner, Borophosphate glasses of the $ZnO–B_2O_3–P_2O_5$ system, Mater. Lett. 42 (2000) 194–199. https://doi.org/10.1016/S0167-577X(99)00183-4.

[55] D. Ilieva, B. Jivov, G. Bogachev, C. Petkov, I. Penkov, Y. Dimitriev, Infrared and Raman spectra of Ga_2O_3-P_2O_5 glasses, J. Non. Cryst. Solids. 283 (2001) 195–202. https://doi.org/10.1016/S0022-3093(01)00361-1.

[56] H. Gao, T. Tan, D. Wang, Effect of composition on the release kinetics of phosphate controlled release glasses in aqueous medium, J. Control. Release. 96 (2004) 21–28. https://doi.org/10.1016/J.JCONREL.2003.12.030.

[57] P.Y. Shih, H.M. Shiu, Properties and structural investigations of UV-transmitting vitreous strontium zinc metaphosphate, Mater. Chem. Phys. 106 (2007) 222–226. https://doi.org/10.1016/J.MATCHEMPHYS.2007.05.038.

[58] Y.M. Moustafa, K. El-Egili, Infrared spectra of sodium phosphate glasses, J. Non. Cryst. Solids. 240 (1998) 144–153. https://doi.org/10.1016/S0022-3093(98)00711-X.

[59] E.A. Abou Neel, W. Chrzanowski, D.M. Pickup, L.A. O'Dell, N.J. Mordan, R.J. Newport, M.E. Smith, J.C. Knowles, Structure and properties of strontium-doped phosphate-based glasses, J. R. Soc. Interface. 6 (2009) 435. https://doi.org/10.1098/RSIF.2008.0348.

[60] T. Kalpana, M.G. Brik, V. Sudarsan, P. Naresh, V. Ravi Kumar, I.V. Kityk, N. Veeraiah, Influence of Al^{3+} ions on luminescence efficiency of Eu^{3+} ions in barium

boro-phosphate glasses, J. Non. Cryst. Solids. 419 (2015) 75–81. https://doi.org/10.1016/j.jnoncrysol.2015.03.033.

[61] B. Glorieux, T. Salminen, J. Massera, M. Lastusaari, L. Petit, Better understanding of the role of SiO_2, P_2O_5 and Al_2O_3 on the spectroscopic properties of Yb^{3+} doped silica sol-gel glasses, J. Non. Cryst. Solids. 482 (2018) 46–51. https://doi.org/10.1016/J.JNONCRYSOL.2017.12.021.

[62] H.R. Ahmadi Mooghari, A. Nemati, B. Eftekhari Yekta, Z. Hamnabard, The effects of SiO_2 and K_2O on glass forming ability and structure of CaO TiO_2 P_2O_5 glass system, Ceram. Int. 38 (2012) 3281–3290. https://doi.org/10.1016/j.ceramint.2011.12.034.

[63] E. Görlich, K. Blaszczak, A. Stoch, G. Siemińska, The devitrification of glasses in the binary system SiO_2-TiO_2, Mater. Chem. 5 (1980) 289–301. https://doi.org/10.1016/0390-6035(80)90027-9.

[64] D. Li, M.E. Fleet, G.M. Bancroft, M. Kasrai, Y. Pan, Local structure of Si and P in SiO_2-P_2O_5 and Na_2O-SiO_2-P_2O_5 glasses: A XANES study, J. Non. Cryst. Solids. 188 (1995) 181–189. https://doi.org/10.1016/0022-3093(95)00100-X.

[65] A.G. Kalampounias, IR and Raman spectroscopic studies of sol–gel derived alkaline-earth silicate glasses, Bull. Mater. Sci. 34 (2011) 299–303. https://doi.org/10.1007/s12034-011-0064-x.

Tables

Table 1. Refractive index (n), Judd-Ofelt parameters (Ω_λ), theoretical (S_a^{th}) and experimental (S_a^{exp}) absolute sensitivities at 473 K.

Sample	n	Ω_2 [10^{-20} cm^2]	Ω_4 [10^{-20} cm^2]	Ω_6 [10^{-20} cm^2]	S_a^{th} a) [% K^{-1}]	S_a^{exp} a) [% K^{-1}]
REF	1.548 ± 0.001	5.5 ± 0.1	3.8 ± 0.1	6.7 ± 0.2	0.0243 ± 0.0006	0.023 ± 0.005
Si-2.5	1.551 ± 0.001	5.6 ± 0.1	4.0 ± 0.1	6.9 ± 0.4	0.0251 ± 0.0006	0.028 ± 0.005
Si-5	1.554 ± 0.001	5.7 ± 0.1	4.2 ± 0.1	9.1 ± 0.5	0.0256 ± 0.0007	0.026 ± 0.005
B-2.5	1.553 ± 0.001	5.7 ± 0.1	4.0 ± 0.1	7.1 ± 0.2	0.0253 ± 0.0006	0.026 ± 0.005
B-5	1.557 ± 0.001	5.7 ± 0.1	4.1 ± 0.1	7.8 ± 0.2	0.0256 ± 0.0006	0.032 ± 0.005

a) at 473 K

Table 2. Temperature of thermal quenching (T_q), quantum yield (QY), theoretically obtained radiative decay time (τ_r) and experimentally measured emission decay time (τ_{exp}) of $^5D_1$ emission, and non-radiative transitions rate (W_{non}).

Sample	T_q [K]	QY_{exp} [%]	τ_r [ms]	τ_{exp} [ms]	W_{non} [s^{-1}]
REF	623 ± 25	44 ± 10	2.92 ± 0.03	2.8 ± 0.1	16 ± 5
Si-2.5	673 ± 25	76 ± 10	2.88 ± 0.03	2.8 ± 0.1	15 ± 5
Si-5	633 ± 25	81 ± 10	2.73 ± 0.04	2.7 ± 0.1	2 ± 7
B-2.5	653 ± 25	105* ± 10	2.78 ± 0.02	2.7 ± 0.1	5 ± 4
B-5	693 ± 25	93 ± 10	2.72 ± 0.02	2.7 ± 0.1	2 ± 4

* the value above 100% is due to the measurement error of 10%. A real value is close to 100%.

Table 3. Density, molar volume and thermal properties of the studied glasses as evaluated through DSC analysis.

Sample	Density ($g\ cm^{-3}$) [± 0.02 g/cm^3]	Molar volume* (cm^3) [± 0.3 cm^3]	T_g (°C) [± 3 °C]	T_x (°C) [± 3 °C]	T_p (°C) [± 3 °C]
REF	2.93	38.1	451	630	672
Si-2.5	2.95	37.1	457	633	696
Si-5	2.98	36.0	462	637	690
B-2.5	2.96	37.1	466	655	710
B-5	2.99	36.2	476	660	738

* Molar volume = molar mass/density